Available online at www.sciencedirect.com
SCIENCE DIRECT®
Physics of the Earth and Planetary Interiors 150 (2005) 159–181
PHYSICS OF THE EARTH AND PLANETARY INTERIORS
www.elsevier.com/locate/pepi

An integrated magnetotelluric and aeromagnetic investigation of the Serra da Cangalha impact crater, Brazil

A.A. Adepelumi[a,*], S.L. Fontes[b], P.A. Schnegg[c], J.M. Flexor[b]

[a] *Korea Institute of Geoscience and Mineral Resources, 30 Gajeong-dong, Yuseong-gu, Daejeon 305-350, South Korea*
[b] *Coordenação de Geofísica, Observatório Nacional, Rua General José Cristino 77, CEP 20921-400, São Cristóvão, Rio de Janeiro, Brazil*
[c] *Institut de Géologie, CH-2007 Neuchâtel, Switzerland*

Received 31 January 2003; received in revised form 28 February 2004; accepted 16 August 2004

Abstract

The research is aimed at delineating the post-impact structural characteristics across the Serra da Cangalha impact crater in Brazil using a combination of magnetotelluric (MT) and aeromagnetic data. The MT survey was carried out along three radial MT profiles trending NW–SE, ENE–WSW and NNE–SSW across the crater. For MT sites located further away from the centre of the crater, isotropic MT responses were observed, suggesting a 1D conductivity distribution in the subsurface in the frequency range of 100–10 Hz. For sites located in the vicinity of the inner ring of the crater, anisotropic responses were observed for the same frequency range. We believe that this zone probably represents the areas of structural disturbance. A 2D resistivity inversion of these data reveals a four-layer model, representing a thin resistive layer underlain by a conductive layer, a weathered basement and a resistive crystalline basement. The depth to the top of the basement is estimated to be about 1.2 km. This is in good agreement with the estimation of depth to the basement of about 1.1 km, calculated using the aeromagnetic data. However, in view of the circular geometry of the crater, we have carried out a 3D forward modeling computation to supplement the derived 2D model. The 3D resistivity forward model, fitting the MT responses by trial-by-error revealed a five-layer model, showing a significant reduction in the basement resistivity. This, perhaps, could be due to the structural disturbances that have been caused by the impact on the crater, resulting in brecciation, fracturing, alteration and shocked zone filled with weak-magnetic materials and fluids. We have calculated the effect of the impact on the overall structural deformation beneath the Serra da Cangalha crater, following the classical crater scaling relation of Holsapple and Schmidt [Holsapple, K.A., Schmidt, R.M., 1982. On the scaling of crater dimensions. II. Impact processes. J. Geophys. Res. 87, 1849–1870] and found to be about 2 km.

Keywords: Impact crater; Magnetotelluric; Aeromagnetic; Basement; 2D resistivity inversion; 3D forward modelling

* Corresponding author. Tel.: +82 42 868 3171; fax: +82 42 861 9721.
E-mail addresses: adepelum@on.br (A.A. Adepelumi), sergio@on.br (S.L. Fontes), pierre.schnegg@unine.ch (P.A. Schnegg), flexor@on.br (J.M. Flexor).

0031-9201/$ – see front matter © 2004 Elsevier B.V. All rights reserved.
doi:10.1016/j.pepi.2004.08.029

1. Introduction

Studies of meteorite impact cratering have been the subject of prime interest, as they facilitate to understand the earth's climatic and biologic evolution in a broader perspective. It is natural that meteorite impacts cause pronounced subsurface structural deformations and produce distinctive changes in the physical properties of the rocks in and around impact structures. These include: (i) changes in the electrical conductivity of the subsurface (Zhang et al., 1988; Amir et al., 2002), (ii) variations in the magnetic field (Hart et al., 1995) and (iii) mineralogical phase changes (Cisowski and Fuller, 1978), to name a few.

Zhang et al. (1988) studied the Siljan impact crater using MT and detected an anomalous upper crust having a resistivity of 1000 Ω m compared to resistivity of 10,000 Ω m found in the adjacent rocks in the region. They invoke the presence of free fluids as suggested by Shankland and Ander (1983), and existence of faults in the lower crust as the most probable source through which this anomaly developed. Mareschal and Chouteau (1990) analyzed MT data over the Charlevoix crater and delineated the existence of a deep vertical conductor and fault beneath the crater. They concluded that the meteorite impact affected the upper 20 km of the crust beneath Charlevoix region. Masero et al. (1994), using MT data, gave a 1D electrical structure of the Araguainha crater in central Brazil. Masero et al. (1995) also provided a 1D geoelectrical model of Serra da Cangalha impact crater and identified a zone of structural disturbances at a depth of 1.1 km beneath the crater, which they used in classifying the Serra da Cangalha as a shallow impact region. Unsworth et al. (2002) delineated a 2D electrical structure of Chicxulub impact crater and reported a significant reduction in the resistivity of the upper crust beneath the crater. They attributed the low resistivity to the result of hydrothermal alteration and mineralization across the ring of the crater in the upper 1–2 km of the crust.

Using magnetic method, the morphological features of various impact craters have been explained in the past. For example, Sturkell and Ormö (1998) derived a bowl-shaped structure of the Lockne crater in Sweden, which has no distinct magnetic anomaly pattern and no melt body. The absence of magnetic signature at this crater is attributed to the presence of great volume of water and wet carbonate rich sediments in the target area. Tsikalas et al. (1998) ascribed the source of the low magnitude (about 100 nT) magnetic signature observed at the Mjølnir Crater located in the Barents Sea to localized dispersed or injected impact-generated melts and/or dislocation of weakly magnetized platform sediments. Plado et al. (2000) carried out a magnetic modeling of the Bosumtwi meteorite impact structure in Ghana. They suggested that the central negative magnetic anomaly (−40 nT) was probably produced by the magnetization of the 400 m thick magnetic lens consisting of impact-melts breccias and impact-melts rocks, and that this magnetic body acquired its bulk remanent magnetization during the Lower Jaramillo normal polarity event.

In all the above studies, it can be understood that while the MT method helps to resolve deep geoelectrical structures, the magnetic method aids to delineate the crater morphology and depth to the basement. Therefore, in an attempt to characterize the Serra da Cangalha impact crater more quantitatively, we, in the present study, have analyzed both MT and aeromagnetic data sets.

2. Geological setting

The Serra da Cangalha meteorite impact crater is located at 46°52′W longitude and 8°05′S latitude in northeast Brazil within the intra-cratonic Parnaiba basin covered by Upper Silurian to Cretaceous sedimentary rocks (Fig. 1). It is the second largest impact crater of the eight known impact craters in Brazil (Crósta, 1987). Its 13 km diameter has been estimated from satellite (Dietz and French, 1973; McHone, 1979) and confirmed by aeromagnetic data sets (Adepelumi et al., 2003).

The Serra da Cangalha impact site consists of thick Palaeozoic sedimentary rocks of Poti sandstone formation. It forms the internal part of the crater and overlies the latest Famennian-Tournaisian subvertical Longá shale formation, which is uplifted by about 400 m from their regional stratigraphic level and is overlain by the Westphalian and younger Piaui sandstone formation (Melo and Loboziak, 2000). The outer edge of the impact structure consists of steep-walled plateaus and mesas, capped by undisturbed level-bedded Permian chert and silty sandstone (McHone, 1986).

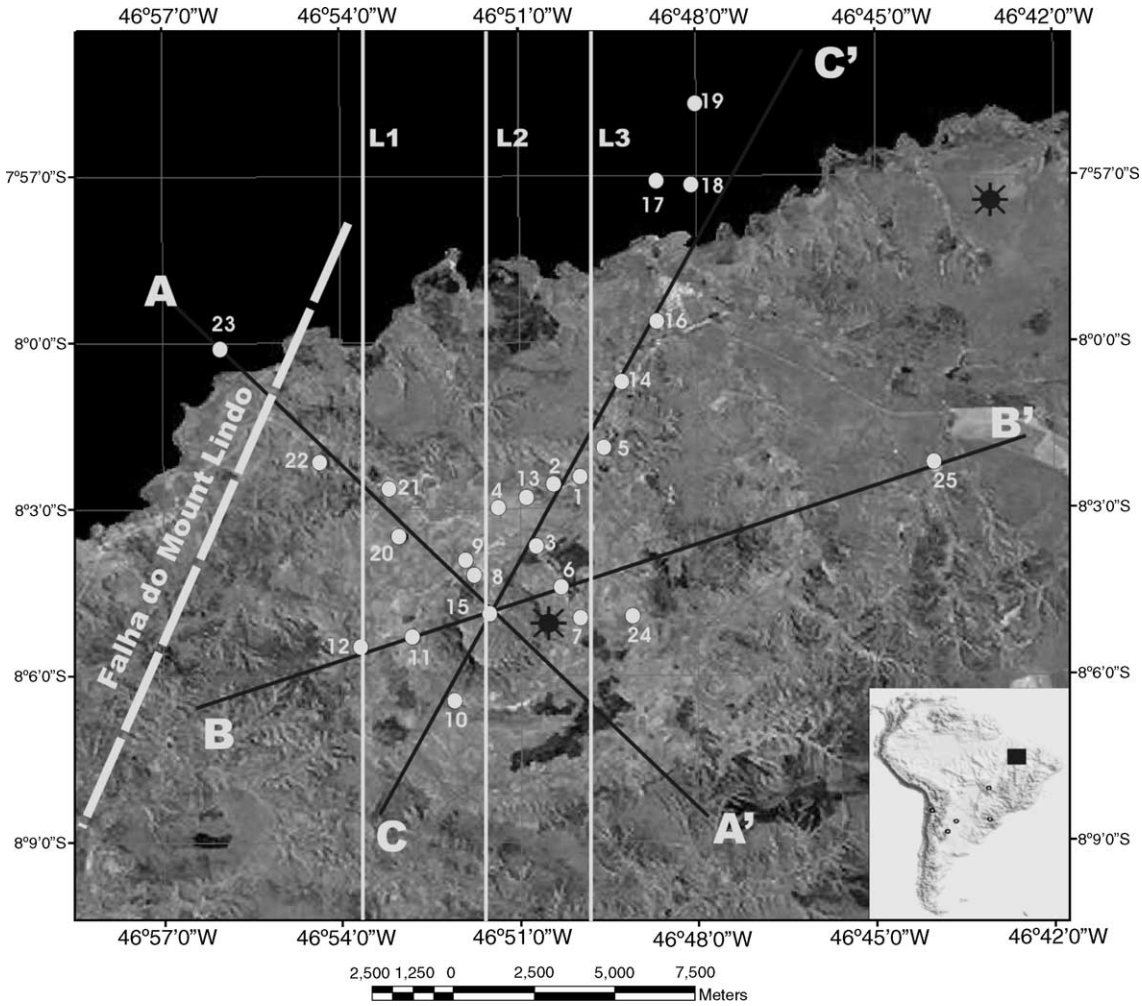

Fig. 1. Landsat image of the Serra da Cangalha impact crater region. The location of the impact crater is indicated with a black filled rectangle superimposed on Brazil map. AA′, BB′ and CC′ shows the profiles used for the magnetotelluric data acquisition. The white circles are the MT sounding sites. Falha do Mount Lindo was extract from the geologic map of the area. The black circles show the locations of the known boreholes in the study area. L1, L2 and L3 designate the three aeromagnetic flight lines.

3. MT data acquisition and processing

In July 1993, MT data were collected at 25 sites along three radial profiles, as shown in Fig. 1. Profile AA′ was aligned in the NW–SE direction, profile BB′ in ENE–WSW direction, and profile CC′ in the NNE–SSW direction. The inter-station spacing is approximately 2 km except for stations 23 and 25 that are far away from possible disturbances caused by the impact. At each site, the simultaneous five-component (three magnetic and two electric) MT measurements in the frequency range of 1030–0.0009 Hz were made using the University of Neuchatel (Switzerland) five-channel system. The soundings were carried out with the telluric lines at each MT station orientated in the direction of the magnetic north and in the corresponding perpendicular magnetic E–W direction. ECA-CM-16 and CM-11-E induction coils (French made) were used for measuring three magnetic components. The MT time-series were processed using standard least square tensorial analysis technique proposed by Sims et al. (1971).

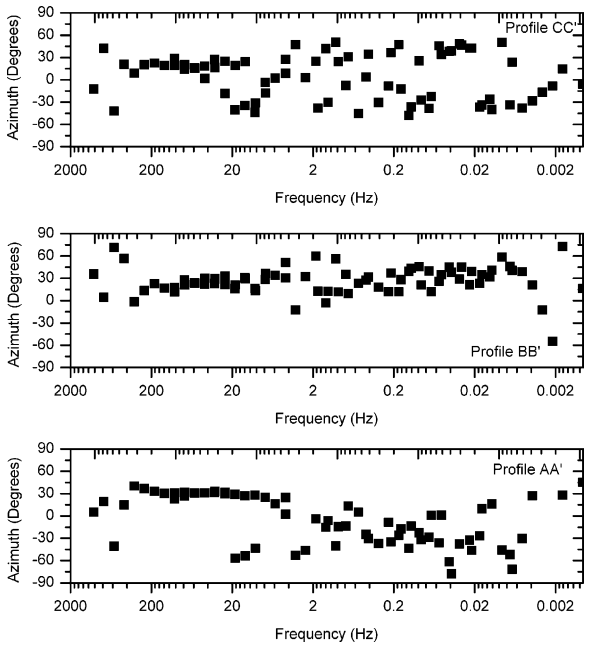

Fig. 2. The regional strike azimuth obtained from the GB multiple-site decomposition of the MT sites along profiles AA′, BB′ and CC′ shown in Fig. 1. This figure displays the representative electrical strike directions found from an unconstrained multi-frequency and multi-site GB decomposition (McNeice and Jones, 2001).

To investigate the influence of near-surface inhomogeneities on the regional inductive responses, we performed both the full tensor decomposition analysis of MT data sets of each station in each profile and jointly for all stations of all the profiles, following McNeice and Jones (2001). The latter exercise was carried out using the unconstrained multi-frequency and multi-site GB decomposition of McNeice and Jones, to determine the best regional strike direction. In both the exercises, the strike angle is found to be well defined only in the frequency range of 200–20 Hz. Fig. 2 shows the representative regional electric strike direction determined to be about N30°E. Considering that the effect of the impact were observed essentially in the high frequency range, we subsequently rotated the data along each profile to the determined regional strike of N30°E.

The galvanic distortion in the Serra da Cangalha impact crater region was examined further in order to understand better the overall distortion levels. Plots of the GB decomposition parameters (twist and shear), found by unconstrained analysis for some sites are shown in Fig. 3a and b. Examination of such plots of all sites indicates that twist and/or shear are well-resolved parameters for almost all the sites. In addition, for most sites located further away from the crater center (e.g. sites 5, 14, 21 and 25), the decomposition yields small twist and shear values, indicating that data in the region are not severely affected by galvanic distortion effects (see Fig. 3a). However, most MT sites (e.g. sites 1, 6, 7 and 15) lying close to inner and outer rings of the crater center present evidence of weak to moderate distortion and minimum electric field polarization (Fig. 3a). The distortion results show that the meteorite impact only produced a moderate electric distortion effects in the high frequency range of 1030–200 Hz of the data sets.

Static shift corrections on MT data were performed as part of the inversion process following the approach of Rodi and Mackie (2001). de Groot-Hedlin (1991) suggested that static shifts may be treated as unknown free parameters during inversion. Also, Gaussian distributions of the static shifts (Ogawa and Uchida, 1996) are assumed. This is a very simple, but reasonable assumption because the static shifts in the data are assumed normally distributed and these distributions have a central mean and well-estimated variance. The inversion program calculates the static shift coefficients and subsequently applies the correction to the data sets where necessary. Fig. 4 shows the apparent resistivity and phase curves for eight of the stations shown in Fig. 1, obtained after GB decomposition.

4. Two-dimensional MT inversion

TE and TM modes data (apparent resistivity and phase) were subjected to regularized 2D inversion of Rodi and Mackie (2001) for a frequency range of 1030–0.01 Hz, along the three profiles, AA′, BB′ and CC′ in Fig. 1. The Rodi and Mackie's inversion technique minimizes both the sum of the χ^2 measure of data misfit and the squared norm of the Laplacian of the model function. We added a minimum noise floor of 5% to the complex impedance to prevent the inversion from being dominated by data with unrealistic variances. Ulugergerli and Candansayer (2002) showed that the accuracy of a 2D MT inversion is affected by both the data quality and the mesh design. They also stated that the dimensions of the grid cells must be kept small compared to the skin depth, so that the obtained

numerical solution may be valid. We therefore chose a very fine mesh for the modeling so as to take care of any lateral variation of the conductivity distribution in the region. For the profile AA′, the mesh is made of rectangular cells having 212 columns and 46 rows; the profile BB′ has 208 columns and 31 rows of rectangular cells and the profile CC′ has 305 columns and 43 rows. The cell thickness gradually increases with depth for all the three profiles.

The relative weight given to the data fit and the model smoothness can be controlled by a trade-off parameter (τ), which controls the inversion result (Rodi and Mackie, 2001). In other words, τ can be viewed as a sensitivity parameter, which essentially controls the RMS value between the data and the model. The optimum τ values were obtained in an iterative manner by first choosing a minimum value of 0.2 and increasing by one order in each of the successive iteration. A τ value of 3 was found appropriate for the Serra da Cangalha data set. For values of τ above and below 3, the data fit degraded, resulting in rougher models. We sought a model that represented a compromise between the data fit and the model smoothness by following the procedure of de Groot-Hedlin and Conssable (1990). The

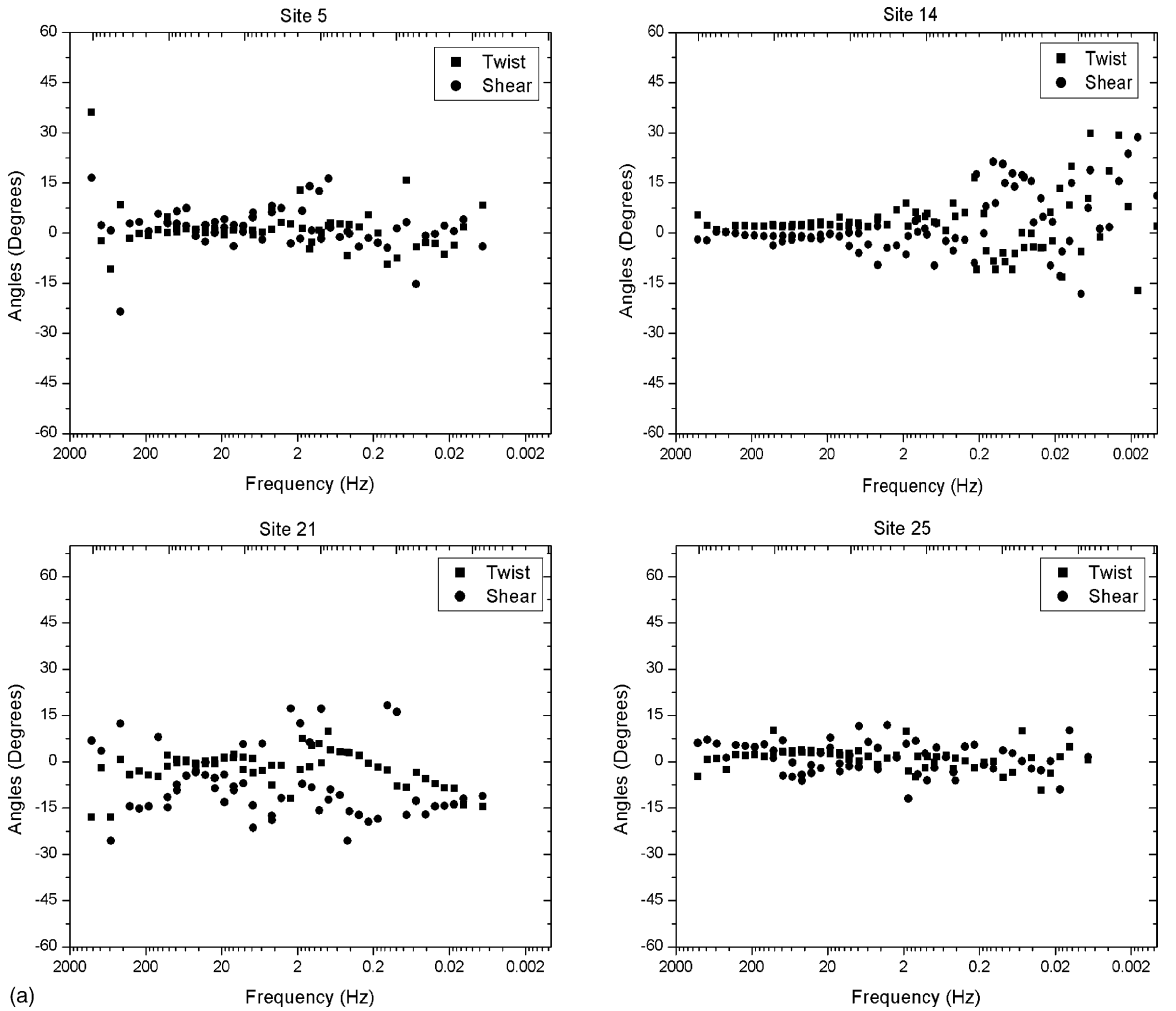

Fig. 3. (a) Distortion parameters determined from the unconstrained GB analysis of MT data of sites 5, 14, 21 and 25 located away from the crater center. (b) Distortion parameters determined from the unconstrained GB analysis of MT data of sites 1, 6, 7 and 15 located close to the center of the crater.

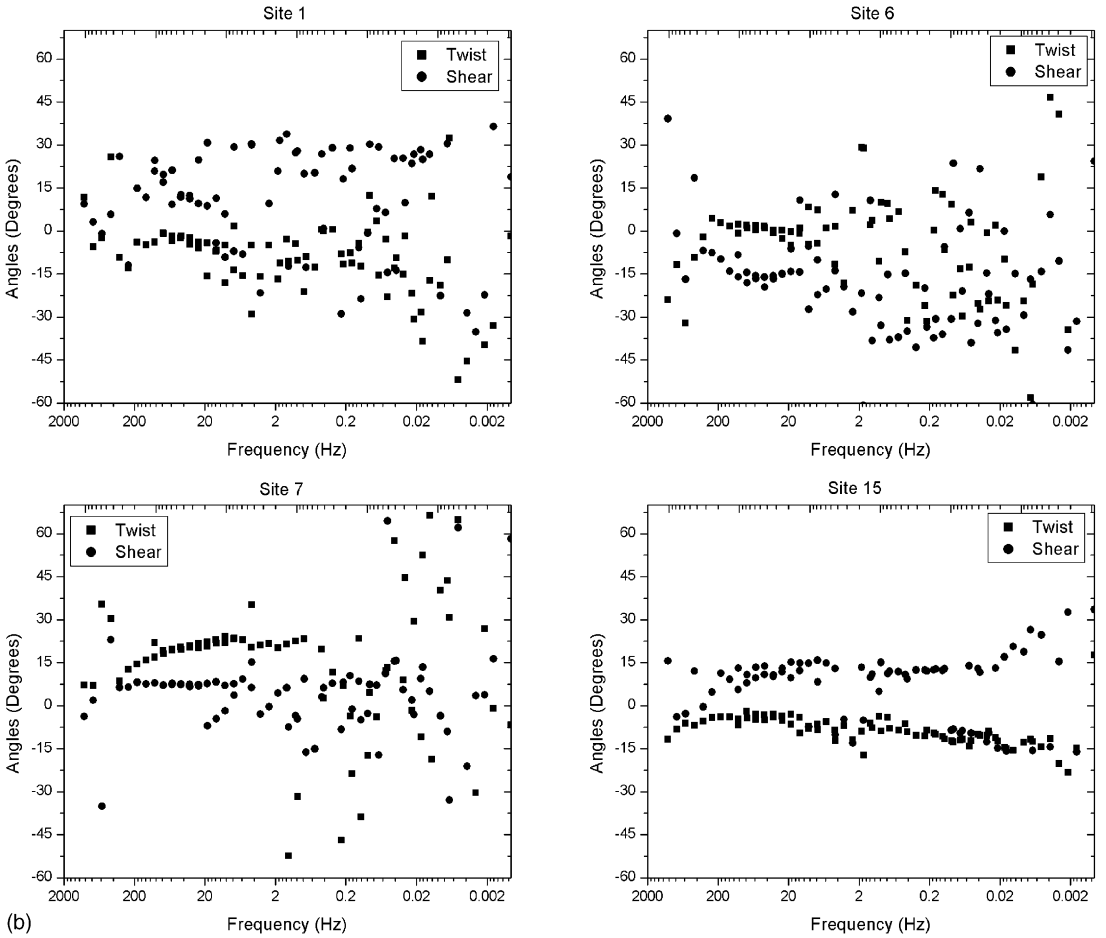

Fig. 3. (*Continued*).

inversion algorithm had converged to constant RMS levels of 2.17 for profile AA′, 2.67 for profile BB′ and 2.57 for profile CC′ after 163 iterations of each profile. Three factors might account for the high RMS errors in the inversion: (i) poor choice of τ values, (ii) the noise unaccounted for by the least square time-series processing, and (iii) the non-2D nature of some of the sounding data.

As well known, 2D model usually yields an appropriate preliminary interpretative approach for 3D geological conditions in the study area. In order to find which 2D model is well resolved, we computed a sensitivity matrix containing the partial derivatives of the data with respect to the model parameters, as proposed by Jupp and Vozoff (1975) and more recently by Schwalenberg et al. (2002). They suggested that the sensitivity matrix should be used to define model parameters that are less resolved by the data and thus should not form a part of interpretation. The results of the sensitivity analysis are presented in Fig. 5a–c corresponding to AA′, BB′ and CC′ profiles respectively. In these figures, the dark gray colour indicates the maximum sensitivity while light gray indicates the minimum. As expected, a general decrease in the sensitivity with depth is observed along the entire 2D sensitivity matrix map. The structural information obtained from the sensitivity analysis is that, of the chosen model, the sensitivity decreases more rapidly with depth. The model parameters that we chose appear to be sensitive, up to a depth of about 2 km (see Fig. 5a–c). Also, the conductive Devonian/Silurian sediments are well resolved beneath all the MT stations. We conclude that

the layers obtained in the 2D model are well resolved. Nevertheless, the 2D model results that were obtained may be one possibility from a multidimensional model space, since the inversion problem remains non-unique.

The TM-mode data fit reasonably well, while misfits are more pronounced in the TE mode. Wannamaker et al. (1984) have shown that it is best to interpret only the TM mode for data along profiles approximately normal to strike, since the TM mode is sensitive to horizontal conductors in resistive hosts. The cause for more misfits in TE mode is perhaps due to 3D effects of off-profile structure. However, we observed that a joint inversion of TE and TM modes yielded a better fit. Therefore, we discuss the joint TE and TM inversion model results only. The final 2D model obtained by jointly inverting the distortion corrected TE and TM modes data are shown in Fig. 6a–c for profiles AA′, BB′ and CC′, respectively. The 2D models show fundamental structural characteristics of the Serra da Cangalha impact crater.

In all the figures, the derived resistivity structure clearly shows four main lithological features. The uppermost layer is a thin resistive layer (about 100 m) constituted by sandstone mixed with sheets of chert nodules and silica-cemented conglomerates (see McHone, 1986); the second layer consists of the combined Devonian and the Devonian/Silurian conductive sediments; the third layer is probably the weathered

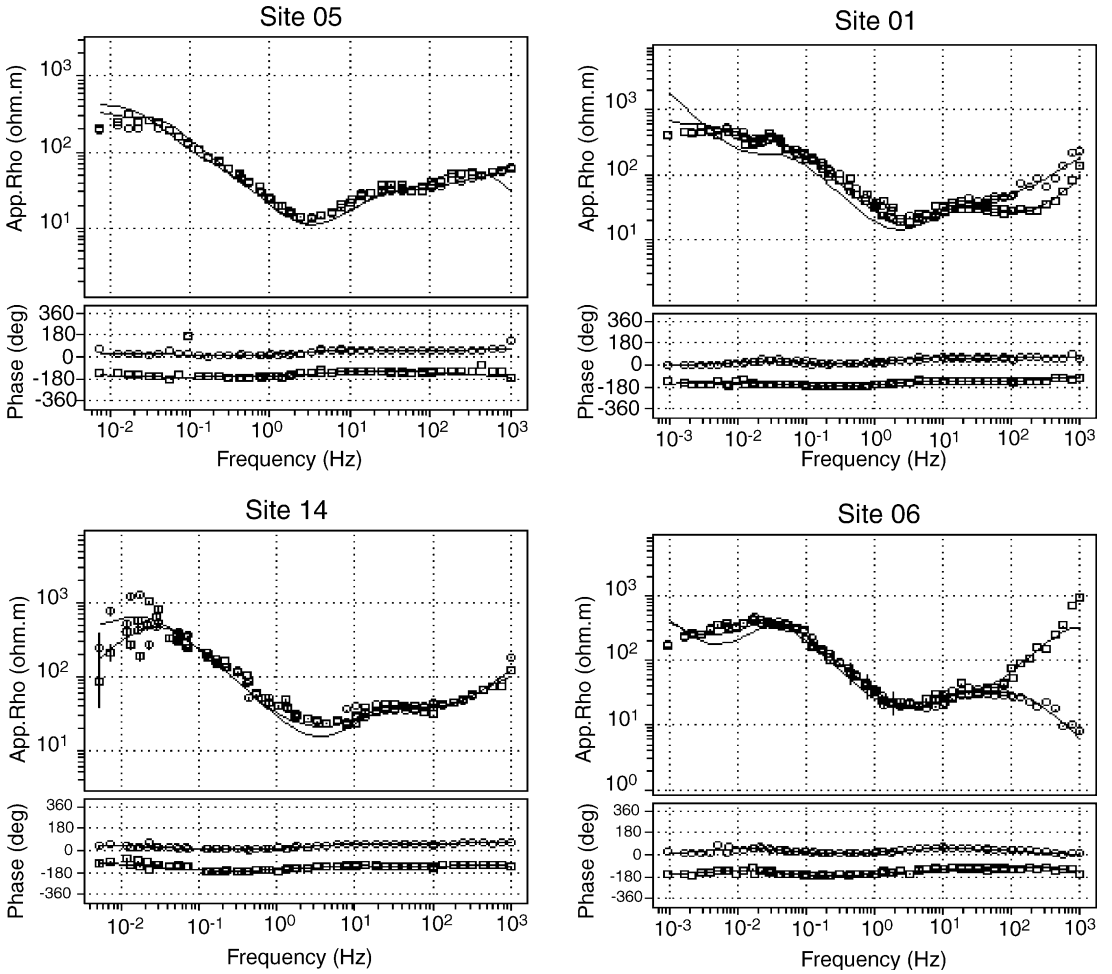

Fig. 4. Examples of apparent resistivity and phase curves calculated from the impedance tensor after rotation to the direction of the regional strike. The panels on the left are MT sites located away from the crater center. The right panels are MT sites located close to the crater center.

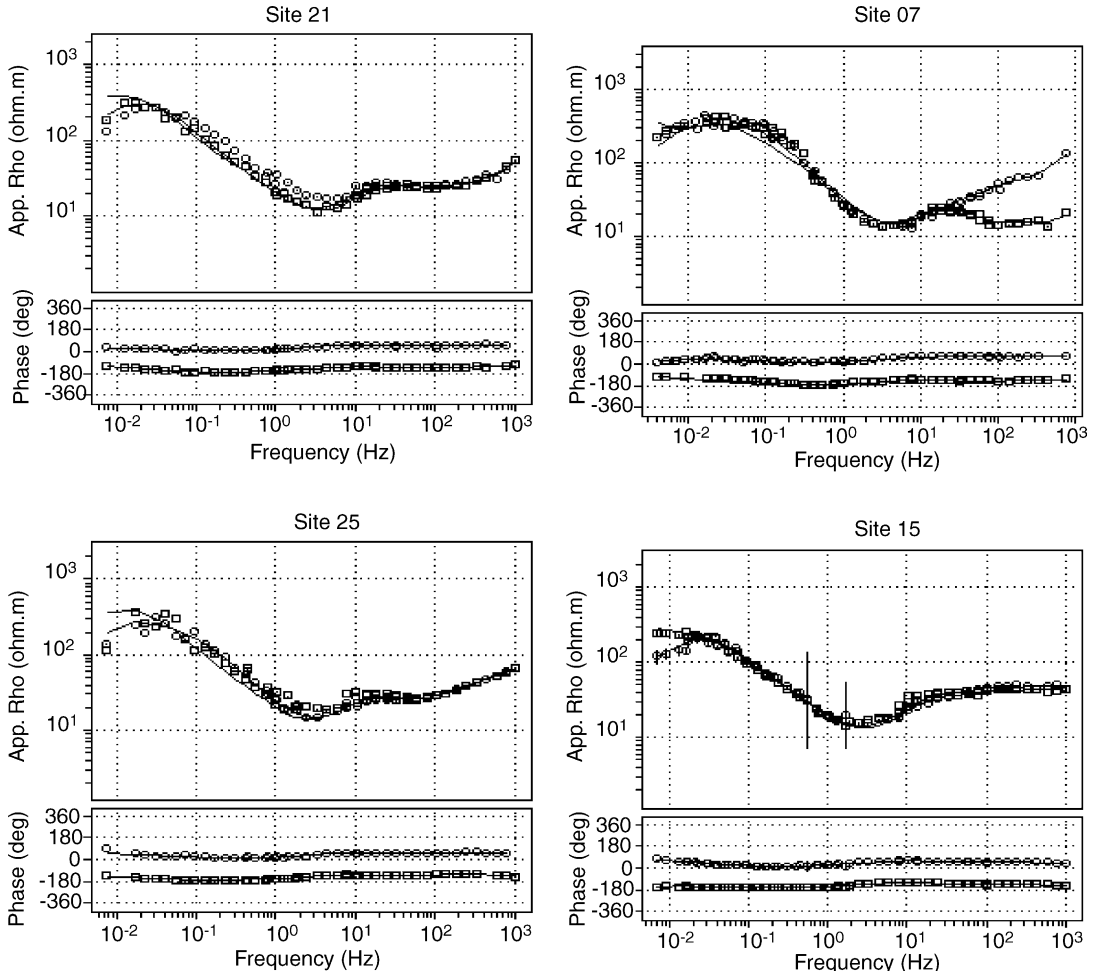

Fig. 4. (*Continued*).

basement, while the fourth layer is the crystalline basement. According to McHone (1986), the conductive layer (labeled B) has been uplifted by about 400 m from their regional stratigraphic level compared to the position of the same formation found in the two Petrobras wells (Mesner and Wooldridge, 1964) located a few kilometers away from the centre of the crater. The uplifted strata were also subjected to intensive erosion (McHone, 1986). Also, the base of these conductive sediments is well resolved along all the three profiles. The conductive layer correlates with the Canindé group comprising of Longá, Cabeças, Pimenteiras and Itaim sedimentary units with alternating sequence of shale and sandstone encountered in Petrobras wells. The resistivity of this layer varies between 10 and 30 Ω m across the entire crater. The thickness of the sediments obtained along all profiles is about 1200 m, which correlates well with the thickness given by an isopach map obtained by Cunha (1986) for Serra da Cangalha region using several data sets of Petrobras wells.

Examination of 2D structures beneath all the profiles show the presence of slump zones, characterised by a series of down-faulted blocks and the uplifted unit (labeled as B) in the northwestern sector of the crater, only beneath the profile AA′ (Fig. 6a). This could be due to the fact that this profile is perpendicular to the regional strike. Therefore, we concentrate discuss on the 2D model results of the profile AA′ only. On AA′ profile, there is an abrupt termination of the conductive layer between MT sites 22 and 23. We relate this to the

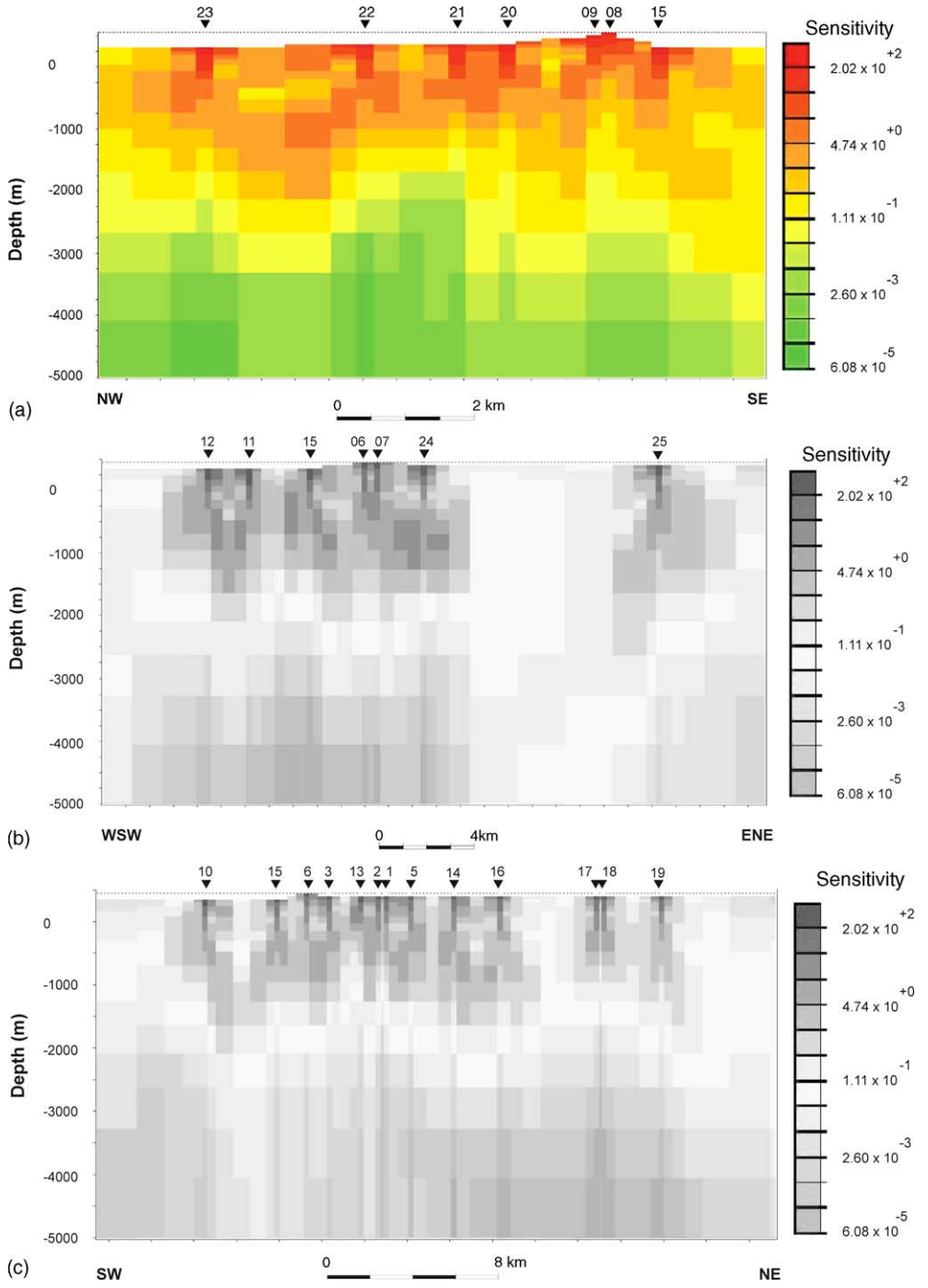

Fig. 5. (a) Sensitivities calculated for the profile AA′ 2D inversion model (joint TE and TM modes). A good resolution is obtained for the shallow structures while the resolution decreases with depth. (b) Sensitivities calculated for the profile BB′ 2D inversion model (joint TE and TM modes). A good resolution is obtained for the shallow structures while the resolution decreases with depth. (c) Sensitivities calculated for the profile CC′ 2D inversion model (joint TE and TM modes). A good resolution is obtained for the shallow structures while the resolution decreases with depth.

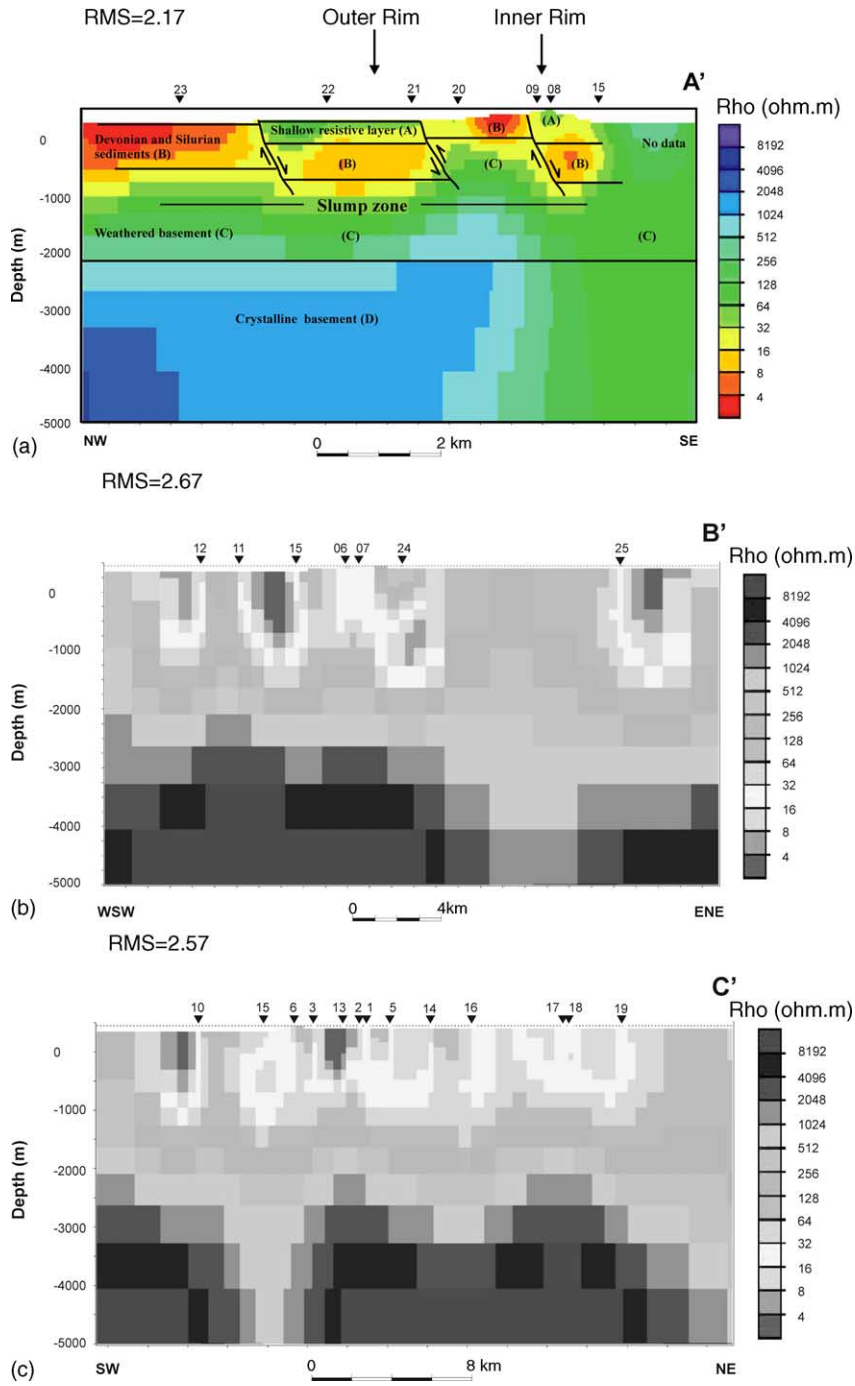

Fig. 6. (a) Final two-dimensional model result that best describes most of the features in the regional MT response along profile AA′ (TE and TM mode data). In the figure above, the notation A, represent the uppermost shallow resistive layer, B represents the conductive Devonian/Silurian sediments, C stands for the weathered basement while D is the crystalline basement. (b) Two-dimensional model result that best describes most of the features in the regional MT response along profile BB′ (TE and TM mode data). (c) Two-dimensional model result that best describes most of the features in the regional MT response along profile CC′ (TE and TM mode data).

fault system called "Falha de Monte Lindo" trending the NE–SW direction (Fig. 1). The base of the conductor extends to a depth range of about 1100 m. The thickness of the conductive sediments also decreases drastically between sites 22 towards 8, i.e., from outer ring to the inner ring (see Fig. 1). Since the sites 8 and 9 are both located on the rim of the inner ring of the impact structure, an uplifted basement is expected beneath these two sites (see 'B' in Fig. 6a).

5. Three-dimensional MT modeling

Considering the circular geometry of the crater as observed from the geological map and Landsat imagery, 3D MT forward modeling was deemed more appropriate than 2D inversion. A 3D model was constructed using the Geotools model builder, and its forward responses were calculated using the code of Mackie et al. (1994) that was recently modified by (Mackie and Booker, 2002; pers. comm.). The central part of the model covers an area of approximately 35 km × 35 km and involves the main geological outcrop and its adjacent area where we suspect that the meteorite impact might be pronounced. The modelled region was discretized into 60 cells in the north–south direction (*x*-axis) and 60 cells in the east–west direction (*y*-axis), and 17 horizontal layers (Fig. 7) in the *z*-direction (downward) that eventually resulted in 1,79,537 solutions. A priori information used in constraining 3D features have been obtained from the results of 1D modeling carried out by Masero et al. (1995), which suggest the existence of an anomalous radial 3D conductor at depth of 1100 m.

The assumed parameters of the five-layer model are given in Table 1. Two double ring bodies, having resistivities of 100 and 600 Ω m representing the crater, were also embedded within the first three layers. A schematic description of the complete model is shown in Fig. 8. For 3D modelling, we used data for ten frequencies ranging from 0.1 to 1000 Hz from a total of 25 MT sites. Data below 0.1 Hz were neglected because we only intend to image the highest frequency data that we suspected were affected by the meteorite impact. Our goal is to find a simple 3D conductivity model that best explains all the selected MT responses. The preliminary model that describes the major features of the impact crater is presented.

Table 1
Three-dimensional layered earth model parameters

Layer number	Layer thickness (m)	Resistivity (Ω m)
1	200	50
2	400	100
3	600	250
4	800	500
5	Half-space	1000

Two double ring bodies having resistivities of 100 and 600 Ω m that represent the crater, were embedded within the first three layers (see Fig. 8).

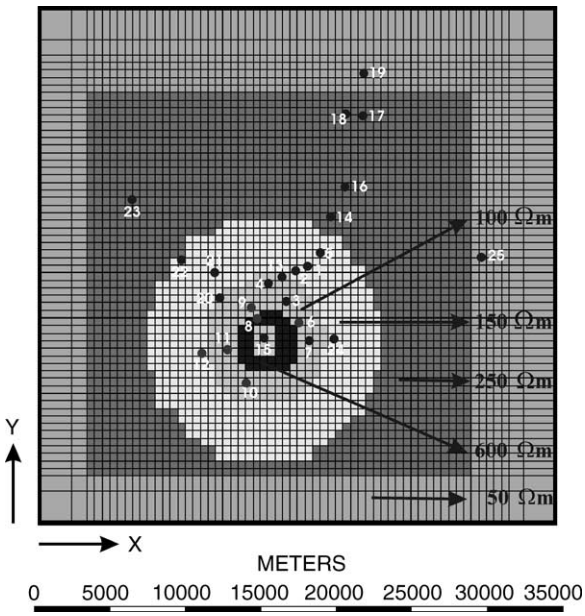

Fig. 7. 3D Mesh generated for the Serra the da Cangalha region. The figure shows the discretised 60 cells in the *x*-axis and 60 cells in the *y*-axis for the first horizontal layer used in the 3D forward modeling. The circular structure at the center represents the impact crater. The black circles are the MT sounding sites.

5.1. Validity of the 3D model results

In order to test the validity of the 3D model itself, prior to estimating the 3D responses, we have selected different models with varying crater dimensions (depth and diameter). The resistivity structure of the five layers model was same in all the models. For models A–C the depth to the base of the crater was fixed at 0.5, 0.8 and 1.1 km and the diameter of the crater was varied be-

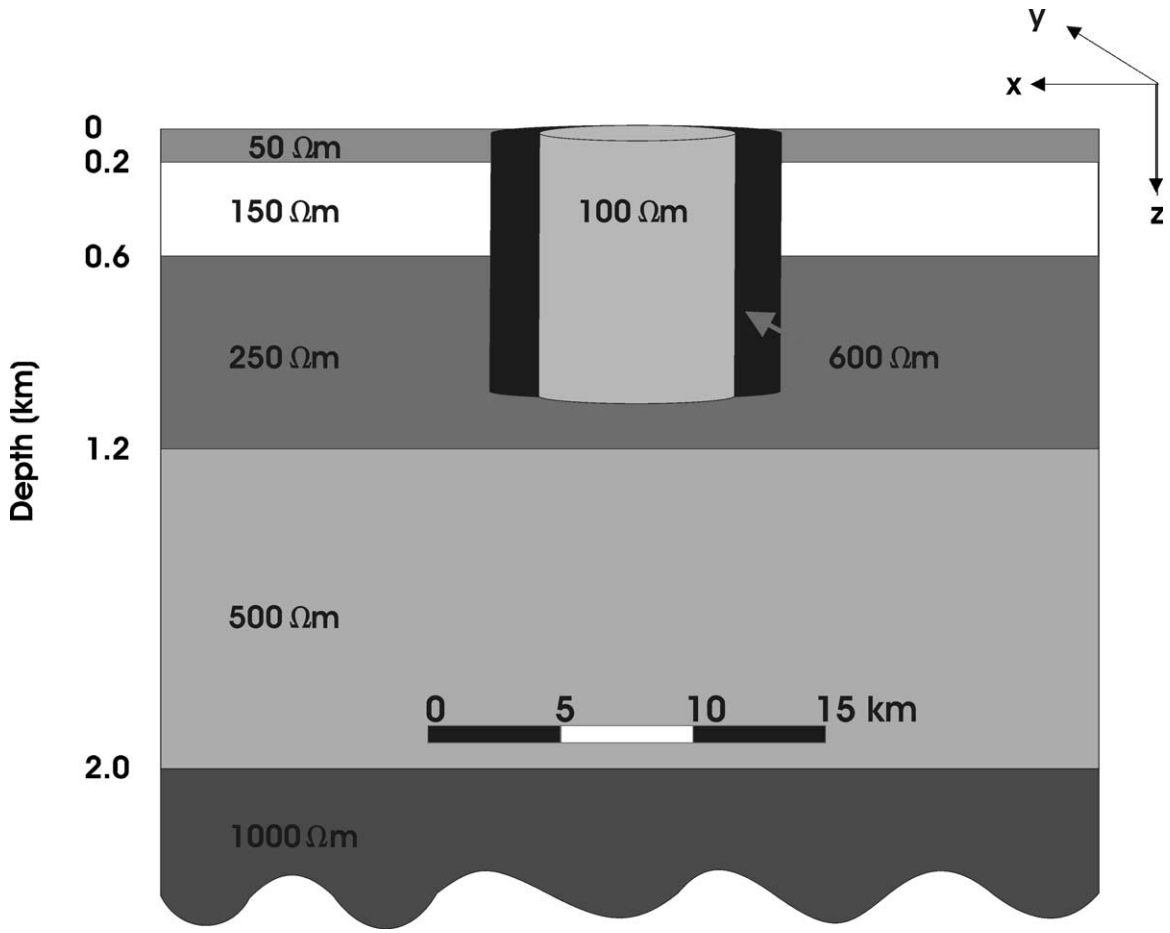

Fig. 8. The conceptual 3D model generated for the Serra the da Cangalha region and painted as vertical slice in geotool.

tween 0.1 and 30 km. In model D, we varied the depth to the base of the crater between 0.1 and 3.0 km while the diameter of the crater was fixed at 13 km. The misfits of the 3D responses were computed in order to confirm the authenticity of the 3D model that we have chosen for this region. The results are shown in Fig. 9a–d.

In Fig. 9 we have plotted the RMS misfit of the 3D model response as a function of the diameter and depth to the base of the Serra da Cangalha impact crater. For models A–C, the misfit was obtained as a result of variation of the diameter (horizontal extension) of the embedded 3D body (crater) while the depth to the base of the crater was fixed at 0.5, 0.8 and 1.1 km. For models A–C, the misfit is smallest and quite stable at a crater diameter of between 11 and 15 km, but it increases steeply when the horizontal extension of the embedded body exceeds 15 km. On the other hand, for crater having a diameter of between 5 and 10.5 km, the misfit also increases but is slightly lower than the misfit obtained for crater having a diameter greater than 15 km. This shows that the model response is not sensitive to these diameters range. This result indicates that 3D models having a crater diameter greater than 15 km are inconsistent with our data because the 3D model responses are very sensitive to changes in the diameter beyond 15 km. Whereas, 3D models having a crater diameter of between 11 and 15 km is compatible with our data. This result suggests that the horizontal dimension of the crater is very important in constraining the 3D model responses. On comparing the misfit between models A with B, we observe that the misfit of model A is about 22% higher than the misfit of model

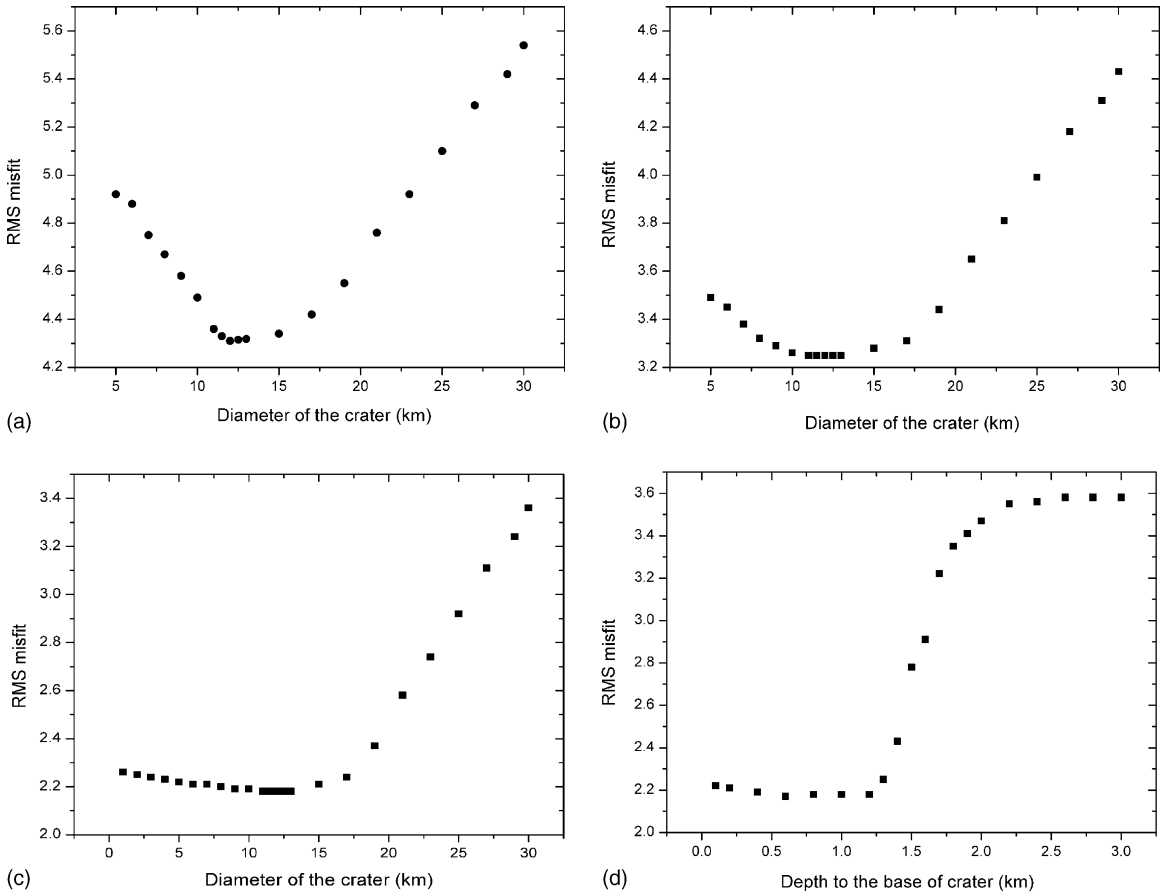

Fig. 9. A plot of the result of the sensitivity tests showing the effect of variation of the diameter and depth to the base of the embedded 3D body on the 3D model responses. In models A–C, the base of the crater was fixed at 0.5, 0.8 and 1.1 km and the diameter varied between 0.1 and 30 km. Whereas in model D, the base of the crater varied between 0.1 and 3.0 km and the diameter was fixed at 13 km.

B, as result, model B is more desirable than model A. Furthermore, a comparison of model B with C shows that the misfit in model B is 26% higher than the misfit in model C. Of all the three models A–C, model C have the lowest and most stable misfit. Therefore, the model C was chosen as the most ideal and realistic 3D model for Serra da Cangalha region.

The results obtained due the variation of depths to the base of the crater is shown in Fig. 9d (model D). From this figure, we observe that the 3D model responses are not very sensitive to changes in the depth to the base of the crater of between 0.1 and 1.2 km. Also, the misfit of this model result is relatively stable at this depth range. However, the fit between the model responses and the observed data significantly worsens beyond 1.2 km. This result reveals that, the depth limits (for the 3D body) causing the anisotropic effects seen on some of our apparent resistivity curves maximally does not extend beyond 1.2 km depth because the lowest misfit and best fits between the modeled and observed data was obtained when the base of the 3D body causing the perturbation was fixed to this depth.

Overall, there is a reasonable agreement between the field data and the model response (apparent resistivities and phases) at all the sites. A split in the curves in the high frequency range characterizes some of the apparent resistivity response curves (Fig. 10). The following inferences could be made from the 3D model result:

(1) The main structure representing the impact crater is well delineated at the centre of the model, suggesting that the impact crater is a relatively shallow tectonic structure that affected the upper 1 km or so of the earth crust. We believe that the 3D character exhibited by the curves is due the heterogeneity of the upper crust, which was probably caused by the meteorite impact.

(2) Between the depth range of 0–600 m, the outer rings of the crater is conductive while the inner ring shows a significant reduction in resistivity with depth until about 1 km depth. This decrease in the bulk resistivity of the inner ring may be explained in terms of the influence fracturing, faulting and brecciation of the rocks in the upper crust caused by the destructive energy and shock waves released by the meteorite on impact as was suggested elsewhere (Amir et al., 2002). Also, the occurrence of the conductive structure seen at the center of the crater is related to the impact-induced altered zone and Paleozoic sedimentary rocks, which are widely distributed in the region. We cannot suggest the presence of mineralization as a possible cause of the low resistivity as is the case of Chicxulub impact crater, Mexico, where an extensive mineralization and hydrothermal alteration of the melts and breccia has been reported (Unsworth et al., 2002). To date, there is no known occurrence of any significant mineralization in the Serra da Cangalha region that could account for the low resistivity observed beneath the crater. Starting from 1.0 km depth, the signature of the inner ring becomes resistive again while the outer ring becomes completely resistive as the regional basement is approached.

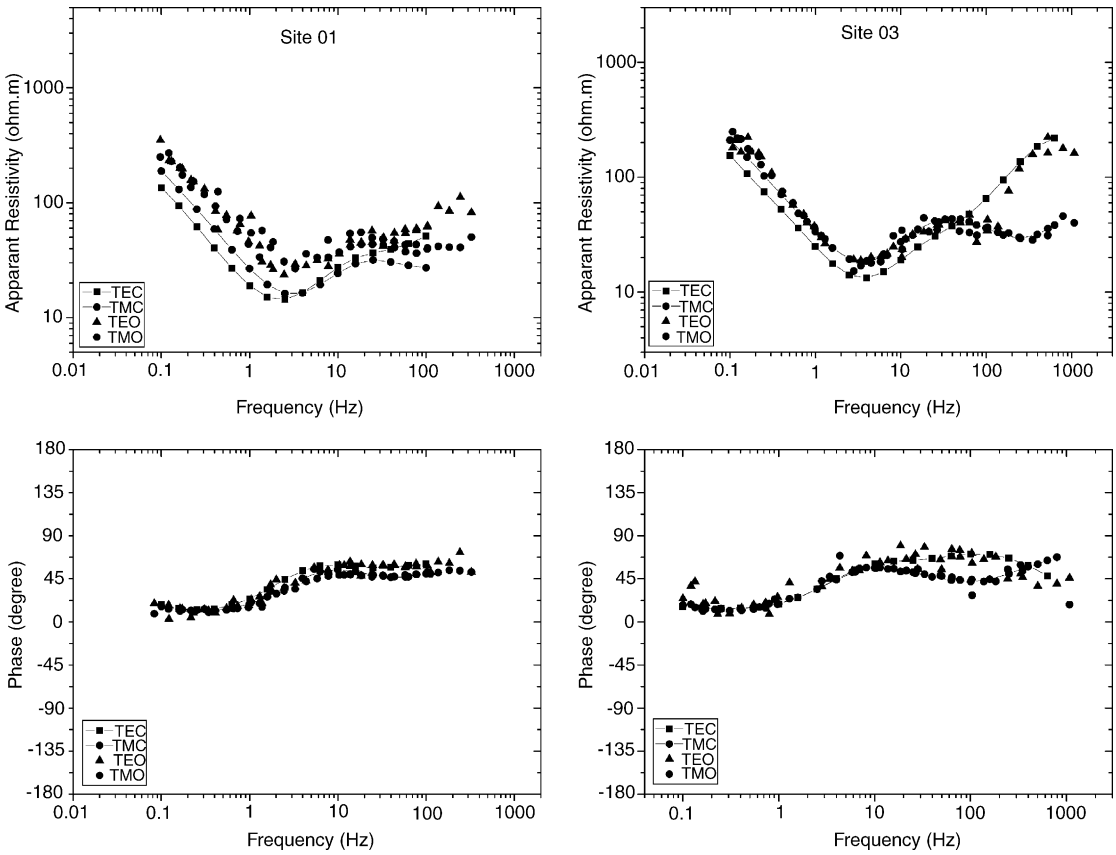

Fig. 10. Comparison of observed (filled triangles and circles) and modeled (open circles and squares) apparent resistivity and phase data at sites 01, 03, 06 and 07. A split of the curves at the highest frequencies characterizes these data, which is indicative of 3D effect.

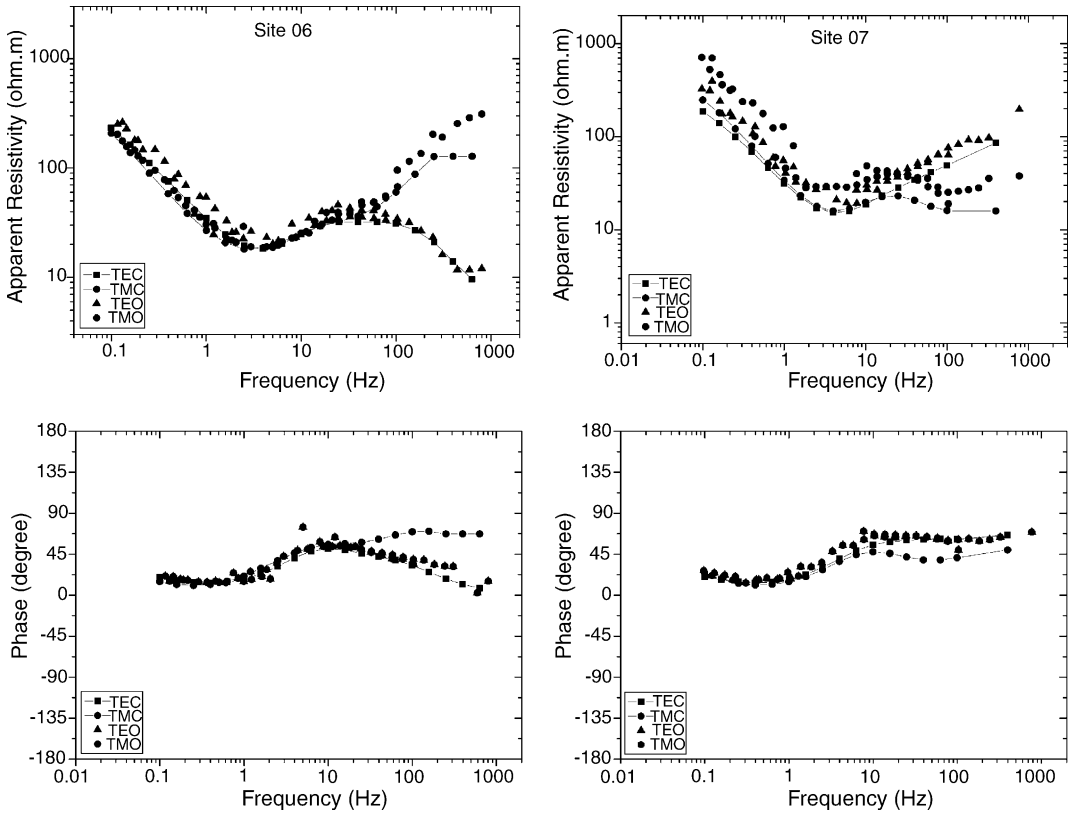

Fig. 10. (*Continued*).

Below this depth, the model becomes more resistive as expected for the crystalline basement. The resistivity increase with depth in the inner ring between 1.0 and 1.8 km can be explained in terms of the intrusion of the uplifted basement into the surrounding sedimentary layers. The main features of the 3D resistivity model presented in Figs. 9 and 10 are consistent with the geology of the region.

It is interesting that this preliminary 3D MT model has enabled us to deduce the post-impact resistivity characteristics of the upper crust that best explain our data. The distinct resistivity contrast of the circular structure revealed by the 3D model may represent an inhomogeneity in the upper crust due to the impact of the meteorite. This might have been formed by considerable impact-induced fractures, microfractures with interconnected pore spaces, and brecciation within the target rocks. Masero et al. (1997), and Zhang et al. (1988) reported a similar occurrence of this low resistivity effect in the upper crust for the Araguainha crater site in Brazil and the Siljan impact region in Sweden, respectively. It was observed that in general, the small dimension of the 3D body modeled has only a small influence on the model response. The 3D structure representing the impact crater is relatively small compared to the regional structure present in the study area.

Masero (1995) and Masero et al. (1995) calculated for each of the 25 MT stations, the induction arrows describing the response of the vertical component of the magnetic fluctuations in order to confirm the probable existence of 3D dimensionality in the study area. They showed that the vertical magnetic fields generally yield induction arrows of very low amplitudes. Also, they reported significant vertical fields in the short periods at the MT sites where splitting of the curves were observed. The induction arrows provide an insight into the conductivity distribution in the subsurface around the Serra da Cangalha impact crater region. They showed that the real part of the Parkinson (1962) induction ar-

rows for 0.1 and 1.0 s point towards the center of the crater. This behavior indicates the presence of a radial conducting structure at this level in the subsurface.

6. Aeromagnetic data processing

The aeromagnetic data was supplied by CPRM (The Brazilian Geological Service). The magnetic flight lines were flown in November 1973 in the N–S direction. They were spaced 4 km apart and tie lines were flown at a spacing of 27 km in E–W direction. A constant clearance altitude of 150 m above the ground level was maintained throughout the survey. The data processing was carried out using the OASIS montaj^{TM}. The total field magnetic map was subjected to IGRF 1973 correction and the main geomagnetic field was removed thereby the residual magnetic fields only were left for further processing.

It is known that geomagnetic field and the magnetization direction of magnetic body are in general not vertical. As a result, magnetic anomalies are typically shifted laterally from the causative body. This usually complicates the interpretation of magnetic anomalies. One way to simplify the shapes of magnetic anomalies, and to translate anomalies so that they are centred directly above the causative body, is to apply reduction-to-the-pole. Therefore, the residual aeromagnetic data were reduced to pole (RTP) using a spectral whitening optimal reduction to pole algorithm (Blakely, 1995). The resulting reduced to pole residual aeromagnetic data were downward continued (Figs. 11–14).

Furthermore, in order to confirm the basement depth across the impact crater obtained through downward continuation, we chose three flight lines that ran across the crater. We calculated the depth by Peter half-slope method (Reynolds, 1998) using the reduced to pole residual magnetic anomaly, obtained along the flight lines. Peter's half-slope method involves finding the maximum slopes of a magnetic anomaly. Through this slope obtained, the depth to the top of the anomaly is calculated.

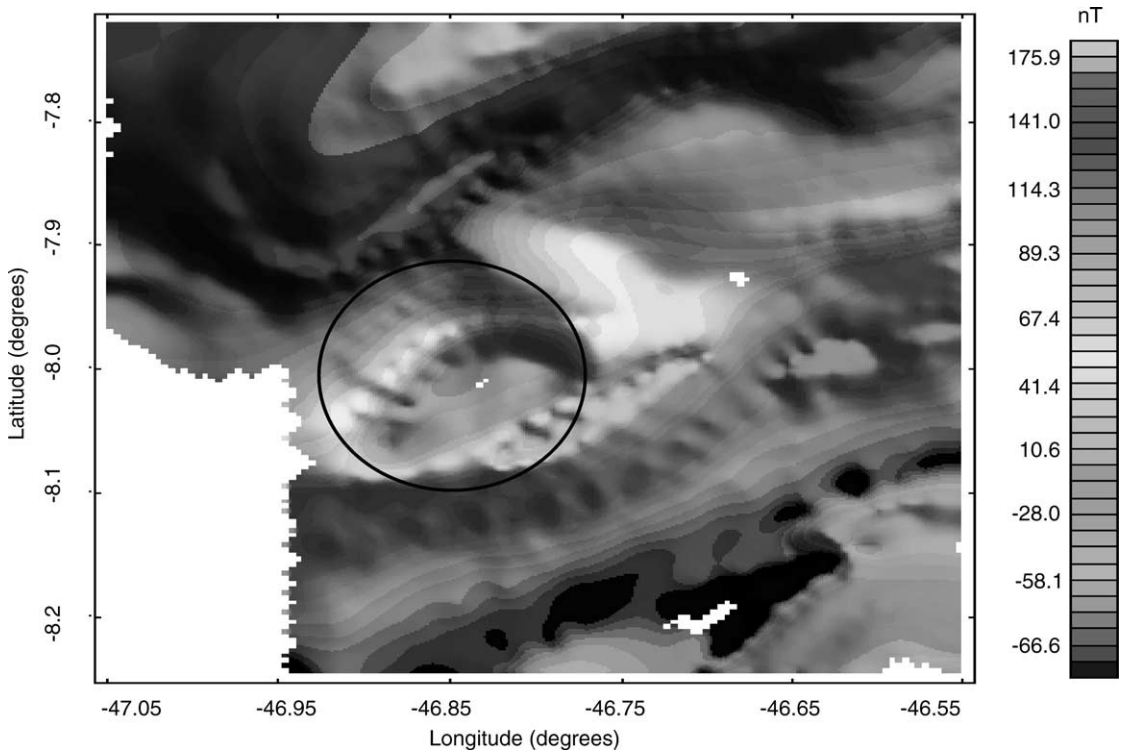

Fig. 11. Aeromagnetic data downward continued to 0.5 km. Note the depression at the centre of the crater. We used the circular ring to delineate the impact crater area. Note the absence of the uplifted basement at this depth.

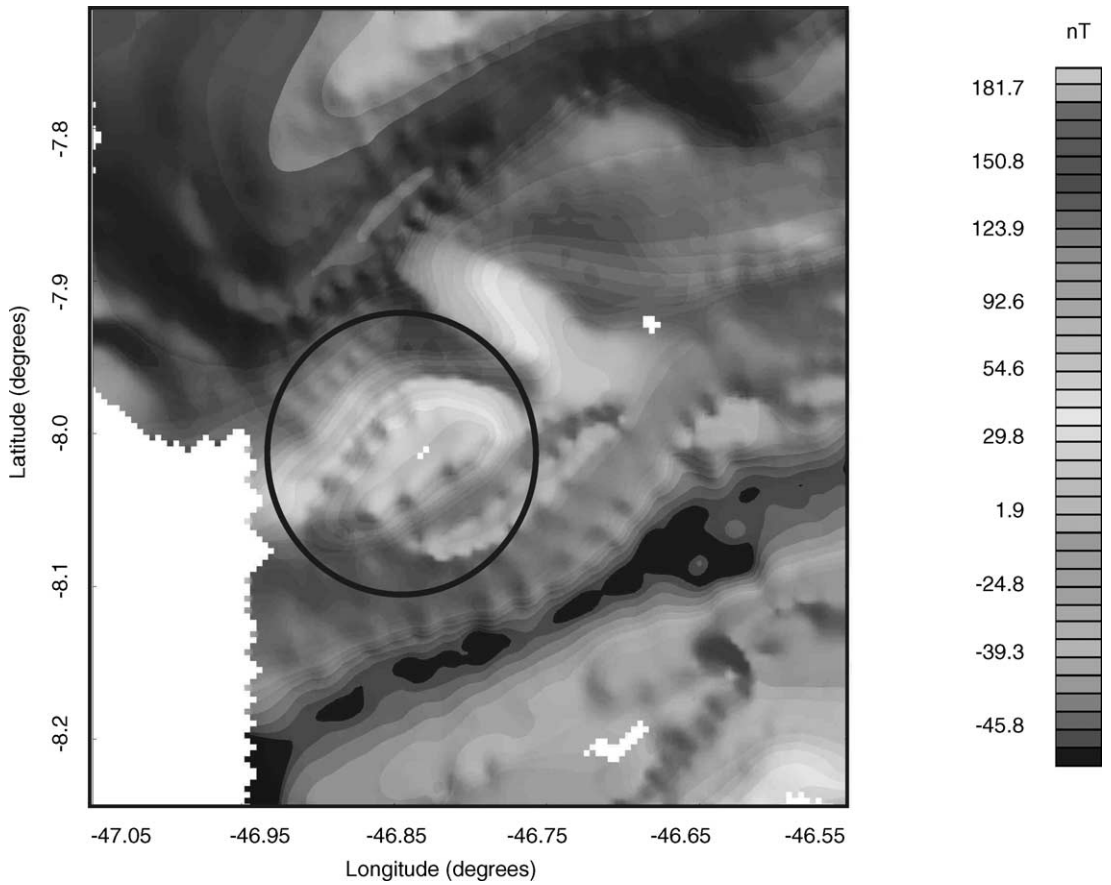

Fig. 12. Aeromagnetic data downward continued to 0.8 km. Note the depression at the centre of the crater. We used the circular ring to delineate the impact crater area. Note that uplifted basement is being approach at this depth.

6.1. Qualitative interpretation of the aeromagnetic data

The impact crater is characterized by: (i) a distinct high positive magnetic anomaly having a relief of 27,400 nT (total field); (ii) bounding low magnetic anomalies to the south (27,267 nT) and (iii) increasing magnetic intensity to the north. In the following section, an attempt has been made to interpret qualitatively the possible causes of the Serra da Cangalha aeromagnetic anomaly, seen in Figs. 11–14. Fig. 11 displays the aeromagnetic data downward continued to 500 m. In this figure, we note that around 500 m depth, we could only observe depression of the sediments. It is evident that the uplifted basement is absent on the shallow downward continued RTP magnetic data corresponding to a layer with a maximum depth of 0.5 km (Fig. 11). In Fig. 12, the same data were downward continued to 800 m, while Fig. 13 shows the downward continued aeromagnetic data to 1100 m depth. From Figs. 12 and 13, the uplifted basement can be clearly seen as the depth of the downward continuation increases from 800 to 1100 m. This structure became clearly visible at 1.1 km depth. This indicates that the source of the magnetic high lies in the top ∼1.1 km and confirms our interpretation of a shallow source. However, below, 1200 m, the uplifted basement disappears (Fig. 14). The 1100 m depth obtained from the downward continuation shows a good correlation with the depth obtained from the 2D inversion and 3D MT modelling shown in Sections 4 and 5.

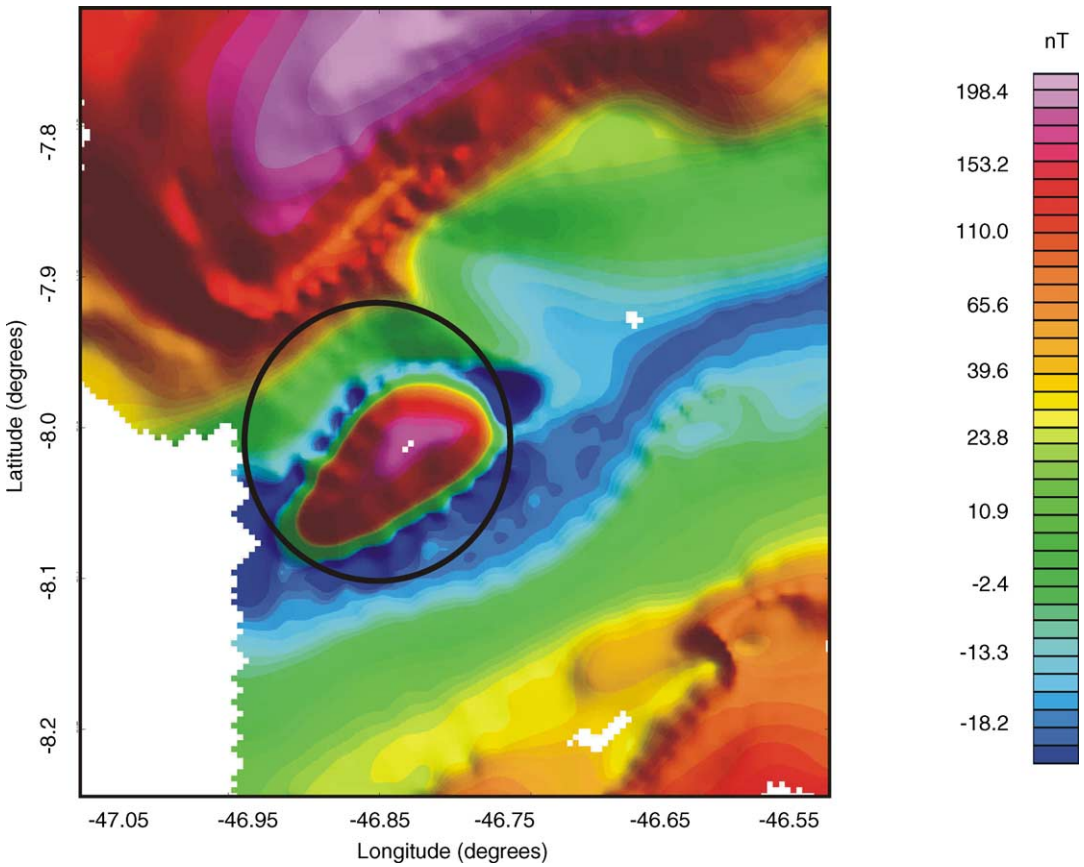

Fig. 13. Reduced to pole residual aeromagnetic map of the Serra da Cangalha impact crater region downward continued to 1.1 km. The circular structure at the centre represents the impact crater region. In comparison with Figs. 15, the uplifted basement is clearly evident from this map.

After applying downward continuation to the aeromagnetic data, the value of the central positive magnetic anomaly was reduced to 152 nT (downward continued to 1.1 km) and the bounding low magnetic anomalies to the south reduced to −18 nT (Fig. 13). This central magnetic anomaly is oval in shape, and striking in the NE–SW direction. Circular shape is expected for the magnetic anomaly. We attribute the oval shape seen in Figs. 11–13 to the large flight line spacing used during the magnetic data acquisition in 1973 and low latitude effect suggested by Blakely (1995). Also, as seen from Fig. 13, the crater tends to align in the NE–SW direction, which corresponds to the regional geology of the region. To the north and south of this structure, the magnetic signature is quite different. The magnetic anomalies in the northern sector of the crater are quite higher than what is obtained in the central crater region; and the magnetic field in the north varies between 155 and 200 nT. Grieve and Pilkington (1996) suggested that craters with a central uplift material and with diameter >10 km tend to exhibit a high-amplitude anomaly. The central positive anomaly observed at Serra da Cangalha area confirmed this suggestion. The delineated uplifted basement explains its formation as a consequence of elastic rebound of the basement structure due to meteorite impact. From this analysis, we are able to confirm that the depth to the top of the body causing the magnetic anomaly seen at the centre of the Serra da Cangalha impact crater.

The results of the depth analysis using the Peter half-slope method are presented in Table 2. The results show that the depths to the basement vary along the three flight lines.

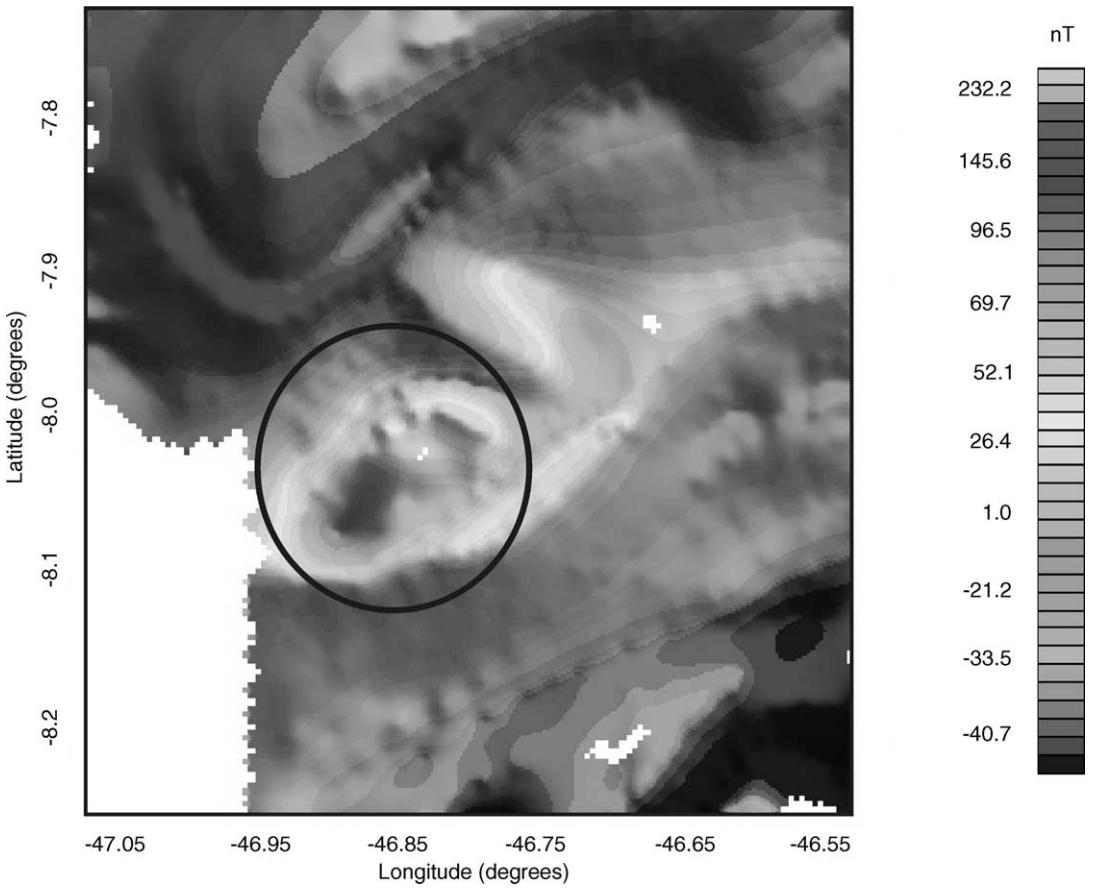

Fig. 14. Reduced to pole residual aeromagnetic map of the Serra da Cangalha impact crater region downward continued to 1.5 km. The circular structure at the centre represents the impact crater region. It is evident that the uplifted basement is no longer well pronounced as in the previous figure.

The magnetic highs observed at Serra da Cangalha impact structure are consistent with observations of structures believed to be caused by meteorite impact in sedimentary terrains around the world, which generally range between tens to hundreds of nanotesla (nT). This magnetic anomaly is the resulting effect of various factors such as the impact angle, impact velocity, strength of the target rocks and the intrinsic strength of the ambient field. We suspect that the central positive anomaly observed at Serra da Cangalha is probably impact related and may have developed as a result of shock demagnetization and shock remagnetization (SRM) acquired at the time of impact as proposed by Wasilewski (1973). Thermal (TRM) and chemical remanent magnetization (CRM) acquired soon after the impact affect target rocks and the formation of remanent magnetization of melts, breccias, footwall complex, post-impact faulting and uplifting of the basement rock. We suggest that the probable occurrence of the various types of remanent magnetizations at the Serra da Cangalha impact region might have contributed to the total magnetic intensity observed in the study area. In addition, Coles and Clark (1982) suggested that the fractured

Table 2
Depth to basement obtained along three flight lines across the crater

Flight lines	Longitude	Latitude	Depth (km)	Error (%)	Remark
1	46°53′46″W	8°05′S	1.9	3.5	Crater centre
2	46°51′46″W	8°05′S	1.2	1.0	
3	46°50′46″W	8°05′S	1.4	2.8	

rocks found around the impact regions are susceptible to chemical alteration resulting from the presence of oxygen and water at post-impact elevated temperatures, which might manifest as a magnetic anomaly over the impact structure. Based on the presence of highly fractured rocks seen around the Serra da Cangalha impact structure (McHone, 1986), we infer that chemical alteration might have also contributed to the positive magnetic anomaly.

Kieffer and Simonds (1980) showed that the volume of melts found in sedimentary craters is about two orders of magnitude less than that for crystalline targets. The reason for this could be due to formation and expansion of large quantities of sediments derived steam like H_2O and CO_2 that resulted in wide dispersion of the shock melted sedimentary rocks and sediment thickness. We believe that the formation of Serra da Cangalha crater in a sedimentary terrain having sediment thickness of up to 3 km might have contributed to the dispersal of the impact-melt shortly after impact. Manson and Lockne impact structures formed in similar environments, as Serra Cangalha shows no defined melt sheets (Sturkell and Ormö, 1998). CPRM (1972) reported a very small melt volume from the boreholes drilled in the area.

According to Melosh (1989) and Morgan and Warner (1997), transient craters are produced during the compressive stage of impact immediately before the gravitational collapse that leads to the formation of the final crater. The excavation craters are formed by the boundary between material that is ejected from the crater and the material that is displaced to form the transient craters. For the purpose of estimating the dimensions of the transient and excavation craters formed at Serra da Cangalha, we have assumed a Maxwell Z-model (Croft, 1980). The maximum depth of excavation (H_{exc}) is given as: $\{(D_{at}/2)(Z-2)(Z-1)^{(1-Z)/(Z-2)}\}$, where D_{at} is the diameter of the transient crater. A Z-value of 2.7 was used. This value has been successfully applied at Ries crater (Hörz et al., 1983) and the Chicxulub crater (Morgan and Warner, 1997). Using the terrestrial scaling laws contained in Melosh (1989), the rim-to-rim diameter of the transient rim uplift was found to be about 6.68 km. The depth of the transient crater was found to be between 1.5 and 2.0 km below the transient crater rim. We derive a maximum depth of excavation of about 0.67 km. The structural implication of the obtained depth of the transient crater is that, impact induced structural deformation from the Serra da Cangalha impact only affected the upper crustal rocks only up to a maximum depth of about 2 km.

According to the morphometric relations given by Grieve and Pilkington (1996) for complex impact structures formed in sedimentary targets, an impact structure with final diameter $D = 13$ km corresponds to a crater with a depth to the top of the breccia lens ($d_a = 0.12D^{0.30}$) of 0.26 km; true crater depth to the

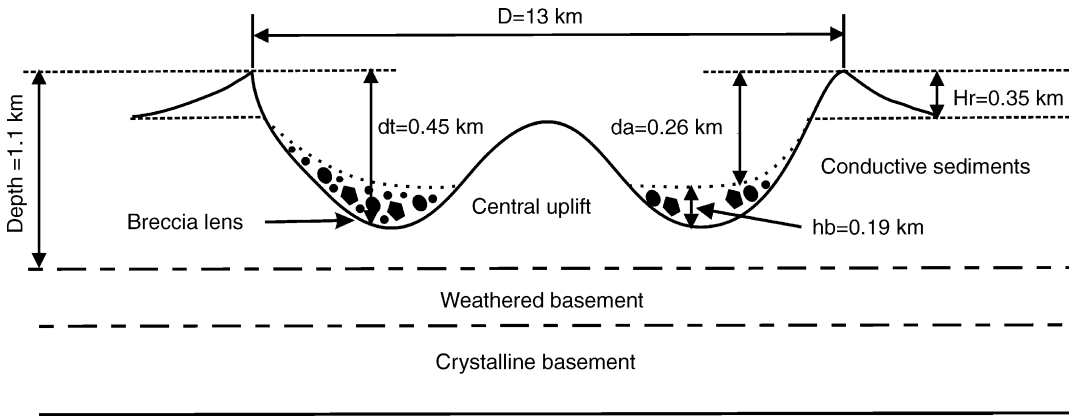

Fig. 15. Schematic diagram illustrating the principal morphometric parameters used to describe Serra da Cangalha impact crater. This model conforms to the norm that says complex impact craters usually have a single or multiple peaks in the middle of the crater. The final crater parameters are given as: D, the rim-to-rim crest diameter; d_t, the rim-to-final crater floor depth; h_r, the crater rim height; d_{cp}, the central crater peak diameter; d_a, depth to the top of the breccia lens; h_b, the breccia lens thickness.

crater floor ($d_t = 0.15D^{0.43}$) of 0.45 km; a maximum central uplift ($0.086D^{1.03}$) of about 1.2 km; and a central peak diameter ($D_{cp} = 0.31D^{1.02}$) of 4.2 km (Fig. 15). McHone (1986) proposed a central uplift of 0.5 km, a central peak diameter of 3.0 km and a true crater depth of 0.34 km deep. However, at the Serra da Cangalha crater site, the available drilled holes reached 200 m depth. For this depth, little trace of breccias was encountered at about 190 m, which is in close agreement with the model apparent crater depth (d_a). Also, the true depth to the crater floor, 0.45 km that we obtained is slightly different from what McHone (1986) proposed. This difference may be due to various factors among which are, deformation, subsidence, gravitation collapse of the transient cavity and tectonic erosion of the crater floor after impact. Geological investigation and remote sensing studies by McHone (1986) placed the height of the crater rim at 350 m. However, using the scaling law proposed for terrestrial impact by Holsapple and Schmidt (1982), we derived ∼360 m as the height of the present crater rim. The two results are in good agreement. Geological studies by McHone (1986) showed that the crater rim is capped by undisturbed level-bedded Permian chert, compact sandstones and silicified fissures. These features are highly resistant materials that prevented the crater rim from being eroded.

7. Conclusions

Two-dimensional resistivity models have been derived by the inversion of the magnetotelluric data from the Serra da Cangalha impact crater region. The three 2D models reveal the post-impact geoelectrical structure beneath the impact crater and show a good conducting layer underlying the area beneath the impact crater. This conductive layer correlates with the Caninde group comprising of Longá, Cabeças, Pimenteiras and Itaim sedimentary units, an alternating sequence of shale and sandstone overlying the basement rock. The depth to basement obtained along profiles AA′, BB′ and CC′ is in good agreement with the information obtained from various Petrobras Oil Company well logs. Also, a normal fault (Falha de Mount Lindo) seen on the geologic map was well delineated. In addition, we suggest that, in order to quantitatively model the Serra da impact structure properly, there is a need to acquire high-quality AMT data in the 1000–10,000 Hz range to better resolve the structures in the top 500 m.

We also characterized structures that probably produced the crater morphology at the Serra da Cangalha impact site with 3D resistivity forward modeling and concluded that the resistivity structure depicts a 3D morphology. The calculated 3D MT response reveals a significant reduction in the basement resistivity around the centre of the crater, which we believe was caused by the impact-induced fracturing of the upper crust. The 3D forward modeling results were very useful in explaining the resistivity behaviour seen at the centre of the crater and provided an insight into the post-impact characteristics of the electrical signature beneath the crater.

We compared the depth to the basement obtained from the 2D MT inversion with the result of the downward continuation of the reduced to pole residual aeromagnetic map to 1.1 km. At this depth, we obtained a distinct central uplift of the basement from the processed magnetic data. A remarkable correlation between both the 2D MT model and the magnetic data suggest that the Serra da Cangalha represents the deep root of a complex impact structure that has undergone differential erosion. The source of the magnetic signatures associated with the central anomaly observed on the aeromagnetic map is suspected to be due to a combination of factors among which are a shock remagnetization (SRM) acquired at the time of impact; thermal (TRM) and chemical remanent magnetization (CRM) acquired soon after the impact. From this study, it was possible to improve our knowledge on the geodynamic structures beneath the impact area through an integrated geophysical study. Future geophysical work on this crater should include the acquisition of a high-resolution magnetic.

Acknowledgements

AAA has been supported by a scholarship from CAPES. We thank Dr. Alan Jones and Dr. McNeiece for releasing their latest version of the tensor decomposition algorithm. Numerous suggestions of the personnel at Geosystem, Italy are immensely appreciated. We thank Maxwell Meju and E. Chandrasekhar for reviewing the manuscript. We also thank

two anonymous referees for helping improving the presentation of this work.

References

Adepelumi, A.A., Flexor, J.M., Fontes, S.L., Schnegg, P.A., 2003. Interpretation of the aeromagnetic signature of the Serra da Cangalha impact crater, Brazil. In: Expanded Abstract of the 8th International Congress of the Brazilian Geophysical Society, (in CD ROM).

Amir, S., Ze'ev, R., Jay, F., 2002. Dynamic fracture by large extraterrestrial impacts as the origin of shatter cones. Nature 418, 310–313.

Blakely, R.J., 1995. Potential Theory in Gravity and Magnetic Applications. Cambridge University Press, 441 pp.

Cisowski, S.M., Fuller, M., 1978. The effect of shock on the magnetization of terrestrial rocks. J. Geophys. Res. 83, 3441–3458.

Companhia de Pesquisa de Recursos Minerais (CPRM), 1972. Relatório de pesquisa de diamante industrial, na região da Serra da Cangalha, estado de Goiás. Ref. DNPM 805.015/70 and 805.019/70, p. 17 (in Portuguese).

Coles, R.L., Clark, J.F., 1982. Lake St. Martins impact structure, Manitoba, Canada: magnetic anomalies and magnetizations. J. Geophys. Res. 87, 7087–7095.

Crósta, A.P., 1987. Impact structures in Brazil. In: Pohl, J. (Ed.), Research in Terrestrial Impact Structures. Vieweg & Sons, Wiesbaden, pp. 30–38.

Croft, S.K., 1980. Cratering flow fields: implications of the excavation and transient expansion stages of crater formation. In: Proceedings of the 11th Lunar Planetary Science Conference. Pergamon Press, New York, pp. 2347–2378.

Cunha, F.M.B., 1986. Evolução Paleozóica da Bacia do Parnaíba e seu arcabouço tectônico. Master's Dissertation. Universidade Federal do Rio de Janeiro, Brasil, 107 pp.

de Groot-Hedlin, C., 1991. Removal of static shift in two dimensions by regularized inversion. Geophysics 56, 2102–2106.

de Groot-Hedlin, C., Constable, S.C., 1990. Occam's inversion to generate smooth, two-dimensional models for magnetotelluric data. Geophysics 55, 1613–1624.

Dietz, R.S., French, B.M., 1973. Two probable astroblemes in Brazil. Nature 244, 561–562.

Grieve, R.A.F., Pilkington, M., 1996. The signature of terrestrial impacts. J. Aust. Geol. Geophys. 16, 399–420.

Hart, R.J., Hargraves, R.B., Andreoli, M.A.G., Tredoux, M., Doucouré, C.M., 1995. Magnetic anomaly near the center of the Vredefort structure: implications for impact related magnetic signatures. Geology 23, 277–280.

Holsapple, K.A., Schmidt, R.M., 1982. On the scaling of crater dimensions. II. Impact processes. J. Geophys. Res. 87, 1849–1870.

Hörz, F., Ostertag, R., Rainey, D.A., 1983. Bunte Breccia of the Ries: continuous deposits of large craters. Rev. Geophys. Space Phys. 21, 1667–1725.

Jupp, D.L.B., Vozoff, K., 1975. Stable iterative methods for the inversion of geophysical data. Geophys. J. R. Astron. Soc. 42, 957–976.

Kieffer, S.W., Simonds, C.H., 1980. The role of volatiles and lithology in the impact cratering process. Rev. Geophys. Space Phys. 18, 143–181.

Mackie, R.L., Booker, J., 2002. Personal communication.

Mackie, R.L., Smith, J.T., Madden, T.R., 1994. Three-dimensional electromagnetic modeling using finite difference equations: the magnetotelluric example. Radio Sci. 29, 923–935.

Mareschal, M., Chouteau, M., 1990. A magnetotelluric investigation of the structural geology beneath Charlevoix Crater, Quebec. Phys. Earth Planet. Interiors 60, 120–131.

Masero, W., Fischer, G., Schnegg, P.A., 1997. Electrical conductivity and crustal deformation from magnetotelluric results in the region of the Araguainha impact, Brazil. Phys. Eart and Planet. Int. 101, 271–289.

Masero, W., 1995. A study of meteoritic impact craters with magnetotelluric method. Ph.D. Thesis. Université de Neuchâtel, Switzerland, 165 pp.

Masero, W., Fontes, S.L., Schnegg, P.A., 1995. Magnetotelluric investigation of the Serra da Cangalha impact structure, Brazil. In: Expanded Abstract of the 4th International Congress of the Brazilian Geophysical Society, vol. 2, pp. 664–667.

Masero, W., Schnegg, P.A., Fontes, S.L., 1994. A magnetotelluric investigation of the Araguainha impact structure in Mato Grosso-Goiás, central Brazil. Geophys. J. Int. 116, 377–392.

McHone, J.F., 1986. Terrestrial impact structure: their detection and verification with two new examples from Brazil. Ph.D. Thesis. University of Ilinois at Urbana–Champaign, USA, 210 pp.

McHone, J.F., 1979. Riachao Ring, Brazil: a possible meteorite crater discovered by the Apollo astronauts. In: El-Baz, F., Warner, D.M. (Eds.), Apollo-Soyuz Test Project. Summary Science Report, vol. II: Earth Observations and Photography, Special Publication No. SP-412. National Aeronautics and Space Administration (NASA), pp. 193–202.

McNeice, G.W., Jones, A.G., 2001. Multi-site, multi-frequency tensor decomposition of magnetotelluric data. Geophysics 66, 158–173.

Melo, J.H.G., Loboziak, S., 2000. Visan miospore biostratigraphy and correlation of the Poti Formation (Parnaiba basin, northern Brazil). Rev. Palaeobot. Palynol. 112, 147–165.

Melosh, H.J., 1989. Impact Cratering: A Geologic Process. Oxford University Press, New York, 245 pp.

Mesner, J.C., Wooldridge, L.C., 1964. Maranhão Paleozoic basin and Cretaceous coastal basins, North Brazil. Bull. Am. Assoc. Petr. Geol. 48, 1475–1512.

Morgan, J., Warner, M., The Chicxulub Working Group, 1997. Size and morphology of the Chicxulub impact crater. Nature 390, 472–476.

Ogawa, Y., Uchida, T., 1996. A two-dimensional magnetotelluric inversion assuming Gaussian static shift. Geophys. J. Int. 126, 69–76.

Parkinson, W.D., 1962. The influence of continents and oceans on geomagnetic variations. Geophys. J. R. Astron. Soc. 6, 441–449.

Plado, L.J., Pesonen, C., Koeberl, C., Elo, S., 2000. The Bosumtwi meteorite impact structure, Ghana: a magnetic model. Meteoritic Planet. Sci., 723–732.

Reynolds, J.M., 1998. An Introduction to Applied and Environmental Geophysics. Wiley, pp. 79–83.

Rodi, W., Mackie, R.L., 2001. Nonlinear conjugate gradient algorithm for 2D magnetotelluric inversion. Geophysics 66, 174–187.

Schwalenberg, K., Rath, V., Haak, V., 2002. Sensitivity studies applied to a two-dimensional resistivity model from the Central Andes. Geophys. J. Int. 150, 673–686.

Shankland, T.J., Ander, M., 1983. Electrical conductivity, temperatures and fluids in the lower crust. J. Geophys. Res. 88, 9475–9484.

Sims, W.E., Bostick, F.X., Smith, H.W., 1971. The estimation of magnetotelluric impedance tensor elements from measured data. Geophysics 36, 938–942.

Sturkell, E.F., Ormö, J., 1998. Magnetometry of the marine, Ordovician Locne impact structure, Jamtland, Sweden. J. Appl. Geophys. 38, 195–207.

Tsikalas, F., Gudlaugsson, S.T., Eldholm, O., Faleide, J.I., 1998. Integrated geophysical analysis supporting the impact origin of the Mjølnir Structure, Barents Sea. Tectonophysics 289, 257–280.

Ulugergerli, E.U., Candansayer, M.E., 2002. Automated mesh design for two-dimensional magnetotelluric interpretation codes. J. Balkan Geophys. Soc. 5, 9–14.

Unsworth, M., Enriquez, O.C., Belmonte, S., Arzate, J., Bedrosian, P., 2002. Crustal structure of the Chicxulub impact crater imaged with magnetotelluric exploration. Geophys. Res. Lett. 29, 351–354.

Wannamaker, P., Hohmann, G., Ward, S., 1984. Magnetotelluric response of three-dimensional bodies in layered earth. Geophysics 49, 1517–1534.

Wasilewski, P.J., 1973. Shock remagnetization associated with meteorite impact at planetary surfaces. Moon 6, 264–291.

Zhang, P., Rasmussen, T.M., Pedersen, L.B., 1988. Electrical resistivity structure of the Siljan impact region. J. Geophys. Res. 93, 6485–6501.